Heliyon 10 (2024) e27310

Contents lists available at ScienceDirect

Heliyon

journal homepage: www.cell.com/heliyon

Research article

A parametric study regarding structural design of a bioprosthetic aortic valve by 3D fluid-structure interaction simulations

Yongwoo Kim [a,1], Won Kyung Pyo [b,1], Wan Kee Kim [c], Ga-Young Suh [d], Keonwook Kang [a,*], Seung Hyun Lee [b,**]

[a] Department of Mechanical Engineering, Yonsei University, Seoul, Republic of Korea
[b] Department of Thoracic Cardiovascular Surgery, Severance Hospital, Yonsei University College of Medicine, Seoul, Republic of Korea
[c] Department of Thoracic and Cariovascular Surgery, Yongin Severance Hospital, Yonsei University College of Medicine, Yongin, Gyeonggi-do, Republic of Korea
[d] Department of Biomedical Engineering, California State University, Long Beach, CA, USA

ARTICLE INFO

Keywords:
Aortic valve
Fluid-structure interaction
Hemodynamics
Biomechanics

ABSTRACT

Since the introduction of transcatheter aortic valve (AV) implantation as a viable option, surgical bioprosthetic AVs have recently started incorporating shorter struts considering future valve-in-valve procedures. However, the effect of leaflet coaptation geometry on the longevity of these valves remains unexplored. To address this gap, we performed a finite element analysis on bioprosthetic AVs with varying strut heights using a two-way fluid-structure interaction method. To establish a baseline, we used a standard height based on a rendered platform image of the CE PERIMOUNT Magna Ease valve from Edward Lifesciences in Irvine, CA. Bovine pericardium properties were assigned to the leaflets, while normal saline properties were used as the recirculating fluid in hemodynamic simulations. The physiological pressure profile of the cardiac cycle was applied between the aorta and left ventricle. We calculated blood flow velocity, effective orifice area (EOA), and mechanical stress on the leaflets. The results reveal that as the strut height increases, the stroke volume increases, leakage volume decreases, and EOA improves. Additionally, the maximum mechanical stress experienced by the leaflet decreases by 62% as the strut height increases to 1.2 times the standard height. This research highlights that a low-strut design in bioprosthetic AVs may negatively affect their durability, which can be useful in design of next-generation bioprosthetic AVs.

1. Introduction

Surgical aortic valve replacement (AVR) has long stood as the gold standard for treating patients with severe aortic stenosis or insufficiency. The primary factors influencing prosthetic valve selection were traditionally the life expectancy of patients and the risks associated with long-term anticoagulation. However, current guidelines now strongly emphasize the importance of considering patient preferences [1,2]. Patients increasingly desire to avoid the risks of bleeding and lifelong anticoagulation. This, coupled with the

* Corresponding author.
** Corresponding author.
E-mail addresses: kwkang75@yonsei.ac.kr (K. Kang), henry75@yuhs.ac (S.H. Lee).
[1] Equally Contributed.

https://doi.org/10.1016/j.heliyon.2024.e27310
Received 30 November 2023; Received in revised form 26 February 2024; Accepted 27 February 2024
Available online 6 March 2024

expanded indications for transcatheter aortic valve implantation (TAVI), including the valve-in-valve (ViV) procedure, has led to a broader application of bioprosthetic valves. As the age of patients receiving bioprosthetic valves trends younger, gaining a deeper understanding of the long-term performance of these valves becomes crucial.

To reduce bioprosthetic valve failure, numerous previous studies have been conducted, the majority of which were clinical studies [3,4] because clinical data can effectively provide direct evidence of the long-term performance of bioprostheses. However, the long tracking time, uncontrollable variables, such as individual differences, sudden death of the subject, and ethical issues make the clinical approach difficult. Alternatively, in vitro experimental methods have been studied along with clinical methods. For example, a mock cardiac circulatory system was used to measure the hemodynamics of a valve [5,6]. Additionally, an accelerated mock system was devised to evaluate the expected life of a valve with reduced opening and closing time [7]. These in vitro studies indirectly prove the longevity of the valves. Irrespective of all the merits mentioned above, experimental methods have a major drawback: not being able to directly measure the mechanical stress developed on a leaflet, which is a critical quantity for failure prediction of the leaflet in the view point of mechanics. Computational simulations can play an important role in the study of bioprosthetic valves because they can provide a physics-based understanding of the behavior of bioprosthetic valves in terms of leaflet deformation and stress.

Numerous computational studies have been conducted on the finite element analysis of aortic valves. For example, the leaflet stress distribution was investigated with different aortic valve shapes during the diastolic phase under quasistatic pressure [10–12]. The effect of the graft shape and material properties were investigated on the aortic valve and sinus under diastolic pressure [13]. Dynamic simulations of a full cardiac cycle were performed to investigate the stress distribution on leaflets by applying a time-varying pressure difference between the left ventricle and the aorta with an anisotropic hyperelastic material model [14]. 3 dimensional fluid structure interaction (FSI) simulations were conducted to investigate the hemodynamic and stress distributions on a leaflet with different material models [16–19]. Luraghi et al. compared both structural and 3D FSI simulations and found that the FSI results were more consistent with the experimental results [20]. In this study, the authors propose an optimal height for the valve strut of a bioprosthetic valve by analyzing the effect of strut height on the structural mechanics of the valve leaflet using 3D FSI simulations. The stress is directly related to the number of cycles the bioprosthesis can withstand in the concept of material fatigue. And hence reducing the maximum stress can increase the life span of the bioprosthetic valve and reduce reoperation or reintervention due to valve failure. Six finite element models were prepared by varying the height of the valve, and full cardiac cycle simulations were performed using the fully coupled FSI method. Stroke volume, effective orifice area (EOA), and stress were calculated by changing the strut height.

2. Methods

2.1. Finite element model preparation

The 3D geometry of the 29-mm Carpentier-Edwards PERIMOUNT Magna Ease bovine pericardial bioprosthetic valve (Edwards Lifesciences, Irvine, CA, USA) was obtained using the MDS500 3D scanner (AGE Solutions S.r.l., Pisa, Italy) and then converted into a stereolithography (STL) computer-aided design file (Fig. 1A). The surface model of the valve leaflets was reconstructed using ANSYS SpaceClaim 18.0 (ANSYS, Inc. Canonsburg, PA, USA) (Fig. 1B). Since the surface of valve is directly converted from the points in scanned STL file, the three leaflets do not show perfect geometrical symmetry. We excluded the skirt and stent parts of the bioprosthesis, focusing solely on the leaflet component with a diameter of 25.5 mm, as in previous studies [17,19,21]. The leaflet

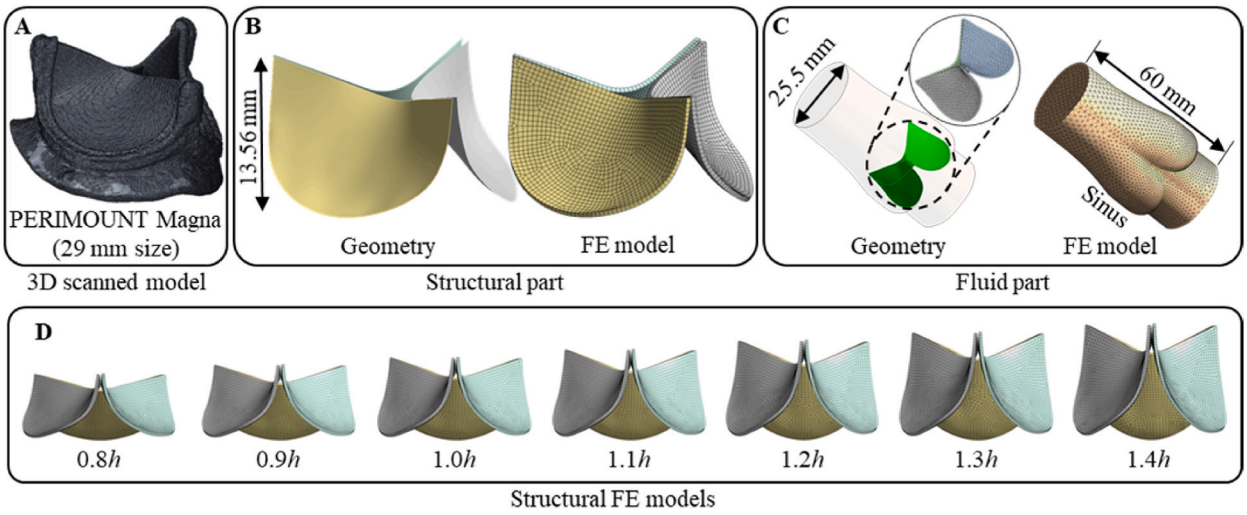

Fig. 1. Finite element model preparation. **A)** 3D scanned stereolithography (STL) model of PERIMOUNT Magna aortic valve; **B)** reverse engineered surface geometry from A and shell-discretized finite element (FE) model of the leaflet for the structural part in fluid structure interaction (FSI); **C)** The fluid domain geometry and FE model for the fluid part in FSI; **D)** structural FE models prepared for parametric study with 0.8, 0.9, 1.0, 1.1, 1.2, 1.3, and 1.4 times the original height of PERIMOUNT Magna, which was $h = 13.56$ mm.

thickness and height were set to 0.5 mm and 13.56 mm, respectively, based on 3D measurements.

To replicate the aortic blood flow, we created a long rigid tube with sinuses at the orifice as the fluid domain. This tube had a length of 60 mm and a diameter of 25.5 mm, consistent with the leaflet size (Fig. 1C). Since solid element requires large number of elements to solve large bending problem of thin material, we discretized the middle surface geometry using first-order four-noded quadrilateral shell elements with full integration for structural simulation. The fluid domain was discretized using second-order 10-noded tetrahedral elements. The leaflet geometry was linearly scaled along the height direction from its lowest point. The height of the reconstructed geometry was varied from 0.8 to 1.4 times the original height (h), at an increment of 0.1h (Fig. 1D). In total, seven finite element (FE) models were prepared to investigate the effect of strut height on the stress experienced by the leaflet. The geometric shape of the sinuses was slightly modified while varying the strut height to ensure a smooth connection. Nonetheless, the rigid tube, housing the leaflets, maintained its original length of 60 mm. Details of the mesh statistics for all the FE models are summarized in Table S1.

2.2. Material properties

The PERIMOUNT Magna Ease aortic valve is a trileaflet valve comprising glutaraldehyde-treated bovine pericardial leaflets. The intact bovine pericardium is composed of collagenous tissue with collagen fibers, which have a preferred orientation and dominant load-bearing components; glutaraldehyde treatment stabilizes the collagenous tissue by adding new inter-fiber cross-links and makes the bovine pericardium anisotropic and hyperelastic [22,23]. Nevertheless, the orientation of collagen fibers was not considered in the manufacturing process. Hence, the authors assumed an isotropic, incompressible, and hyperelastic material model for the bovine pericardium. Uniaxial [24] and biaxial [25] stress-strain curves were reproduced (Fig. S1) and fitted to the Ogden third-order strain energy model for hyperelastic materials, whose strain energy potential W is defined as follows:

$$W = \sum_{i=1}^{3} \frac{\mu_i}{\alpha_i}\left(\bar{\lambda}_1^{\alpha_i} + \bar{\lambda}_2^{\alpha_i} + \bar{\lambda}_3^{\alpha_i} - 3\right) + \sum_{k=1}^{3} \frac{1}{d_k}(J-1)^{2k} \tag{1}$$

where $\bar{\lambda}_1$, $\bar{\lambda}_2$, and $\bar{\lambda}_3$ denote the deviatoric principal stretches, defined as $\bar{\lambda}_p = J^{-\frac{1}{3}}\lambda_p$ for $p = 1, 2, 3$. λ_1, λ_2, and λ_3 are the principal stretches of the left Cauchy-Green tensor. J is the determinant of the elastic deformation gradient, while μ_i, α_i, and d_k denote the material constants to be determined through fitting. The parameters obtained from this fitting process are listed in Table 1. The 2nd term in Eq. (1) was omitted due to the assumption of incompressibility. The density of bovine pericardium was defined as 1120 kg/m^3 [26].

The blood was assumed to be a Newtonian, incompressible and laminar type of fluid, with a density of 1000 kg/m^3 and a dynamic viscosity of 0.004 kg/m-s [16]. In many previous computational studies [15–20,27], the Newtonian model of blood has been adopted in large arteries such as aorta. This assumption is justified by De Vita et al. [28], where they compared the result of non-Newtonian and Newtonian fluids and found that the large-scale flow features were very similar for both fluid models. ***2.3. Boundary conditions***.

In the fluid model, we applied a physiological pressure difference between the left ventricle and aorta at the inlet of the ventricle. At the outlet of the aorta, zero pressure was maintained. The pressure difference curve encompassed both systolic and diastolic phases, starting with the early systolic phase. To derive this pressure difference, we used the Wiggers diagram [29]. The diagram and the pressure difference curve are shown in Fig. 2A and B.

We imposed a no-slip boundary condition on the aortic walls. The leaflets were configured to interact with the structural model, providing calculated nodal forces and receiving nodal displacements to and from the structural solver. In the structural model, the leaflet boundaries were essentially fixed, with tangentially frictionless contact between leaflets. Normal contact was defined using the penalty contact algorithm [30], where the normal contact stiffness is directly proportional to the contact penetration distance raised to the power of three.

2.3. Calculation of effective orifice area

The EOA was determined following the guidelines provided by the International Organization for Standardization (ISO) 5840–1:2021, which outlines general requirements for heart valve substitutes intended for implantation [31]. Equation (2) from ISO 5840–1:2021 was utilized to calculate the EOA, where Δp represents the mean pressure gradient across the valve, and ρ is the fluid density. The calculation of q_{vRMS} (root mean square forward flow rate) in Eq. (2) is derived from Eq. (3), where t_1 denotes the onset of positive differential pressure, t_2 denotes the end of positive differential pressure, and $q_v(t)$ is the instantaneous flow rate [31].

$$EOA = \frac{q_{vRMS}}{51.6 \times \sqrt{\frac{\Delta P}{P}}} \tag{2}$$

Table 1
Parameters (μ_i, α_i) fitted for Ogden 3rd strain energy model in newton meter unit system and normalized root mean squared error (NRMSE).

Parameter	$\mu 1$	$\mu 2$	$\mu 3$	$\alpha 1$	$\alpha 2$	$\alpha 3$	NRMSE
Value	−8708.9	−0.10871	2331.1	−18.088	−54.023	23.533	0.00164

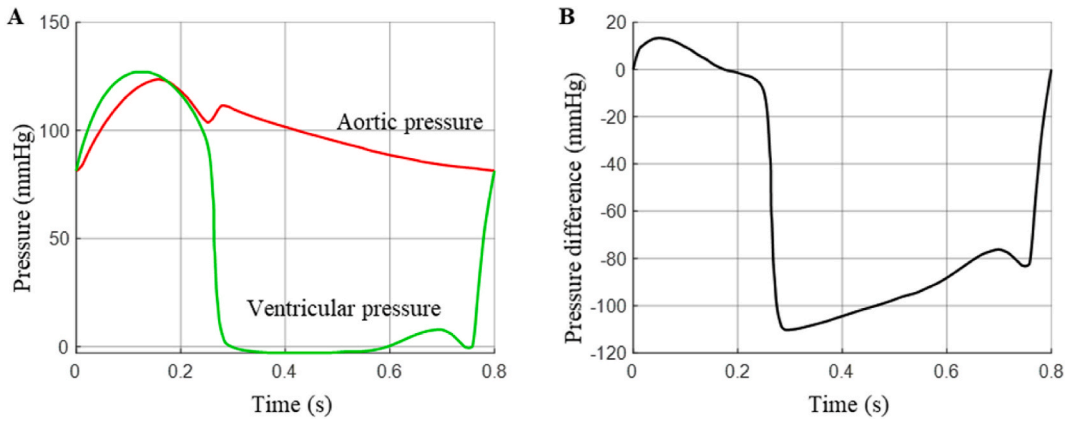

Fig. 2. A) Wiggers diagram illustrating physiological aortic and ventricular pressure during one cardiac cycle; **B)** Pressure difference between aorta and ventricle, applied at inlet of the fluid domain.

$$q_{vRMS} = \sqrt{\frac{\int_{t1}^{t2} q_v(t)^2 dt}{t_2 - t_1}} \tag{3}$$

3. Results

3.1. Flow rate, effective orifice area and maximum valve opening area

The parameters determined in the simulation, such as EOA and allowable leakage, were within the acceptance ranges set by the ISO 5840–1:2021 standard [31]. The volumetric flow rates for all the six FE models in a complete cardiac cycle are illustrated in Fig. S2. The systolic and leakage volumes for each model were computed by integrating the area above and below the *x*-axis of the flow rate curve, respectively. The stroke volume was determined by subtracting the leakage volume from the systolic volume. The values of the systolic, leakage, and stroke volumes are listed in Table 2. The systolic and stroke volumes increased with the valve height, while the leakage volume decreased. Though the leakage volume percentage was slightly higher (11%) than that of a 21 mm-sized valve reported by Dal Lin et al. in an in vitro experiment [32], it remained within the acceptable limits specified by the ISO 5840–1:2021 standard (<20%), considering the larger valve size (29 mm) used in this study.

The EOA was calculated based on the simulation results, using the values Δt (0.1742 s), Δp (8.2632 mmHg), ρ (1 g/cm^3), and the corresponding $q_v(t)$ (mL/s). The EOA for each valve strut height is summarized in Table 2. All the EOA values exceeded the minimum acceptable criterion of 1.95 cm^2 [31]. The EOA increased with higher strut heights, reflecting an increase in q_{vRMS}. For the 29 mm PERIMOUNT Magna Ease aortic valve, a EOA of 2.8 ± 0.5 cm^2 has been reported [33], showing a median value that differs by 5.29% from the results of the present study. The shape of valve opening was represented using orthogonal projection, and the maximum valve opening is shown in Fig. S3. Table 3 summarizes the values of the maximum valve opening area based on the strut height. Although direct comparison in terms of stress distribution and durability is not possible as there are no published data available, our simulation results are indirectly validated by comparing EOA with a clinical value resulting in a difference of 5.29%.

3.2. Leaflet deformation during a cardiac cycle

To visualize the deformation of the leaflet in a cardiac cycle in a region-specific manner, and for ease of analysis, we divided the leaflet into three regions based on the height of the initial geometry, as depicted in Fig. S4. The temporal deformation of the model with the original height (1.0*h* model) was represented through color mapping of the induced maximum principal stress (σ_1), as shown in

Table 2
Calculated systolic, leakage, stroke volumes and effective orifice area (EOA) according to valve height ($\rho = 1$ g/cm^3, $\Delta p = 8.2632$ mmHg, $\Delta t = 0.1742$ s) The leakage volume percentage in parenthesis was obtained based on the corresponding systolic volume.

Height	Systole vol. (mL	Leakage vol. (mL)	Stroke vol. (mL)	$q_{v_{RMS}}$ (mL/s)	EOA (cm2)
0.8*h*	67.25	14.97 (22.3%)	52.28	404.44	2.727
0.9*h*	72.85	13.26 (18.2%)	59.59	421.70	2.843
1.0*h*	76.76	12.45 (16.2%)	64.32	437.23	2.948
1.1*h*	78.83	11.87 (15.1%)	66.96	444.52	2.997
1.2*h*	78.06	11.67 (15.0%)	66.39	445.15	3.001
1.3*h*	79.68	11.72 (14.7%)	67.97	453.08	3.055
1.4*h*	80.38	11.07 (13.8%)	69.31	456.08	3.075

Table 3
Maximum valve opening area (cm^2) and highest maximum principal stress value, Max (σ_1) in MPa according to valve height.

Height	Maximum valve opening area (cm2)	Max (σ_1) (MPa)
0.8*h*	2.910	1.6688
0.9*h*	2.962	1.2604
1.0*h*	3.011	1.2314
1.1*h*	2.988	0.6600
1.2*h*	3.032	0.4695
1.3*h*	3.094	0.4904
1.4*h*	3.175	0.5474

Fig. 3. In the early stage of the systolic phase, the mid-region of the leaflet began to exhibit convex bulging, followed by sequential opening of the upper region, which resulted in convex deformation of the middle regions and concave deformation of the lower region. In the diastolic phase, the valve closed from the lower to the upper regions of the leaflet (see Online Movie I). The temporal deformation of each valve leaflet, including 0.8*h*, 1.2*h*, and 1.4*h* models, and their corresponding maximum principal stress contours are presented in Fig. 4A–C and Online Movie II.

Supplementary video related to this article can be found at https://doi.org/10.1016/j.heliyon.2024.e27310

3.3. Induced stress according to the valve height

The maximum principal stresses (σ_1) across the entire valve region were monitored during the simulations, and the highest value in the cardiac cycle was plotted over time for the seven different models in Fig. 5A. The highest σ_1 value decreased when the valve height increased from 0.8*h* to 1.2*h* and then increased again when the valve height exceeded 1.2*h*.

Fig. 5B-D shows the highest stress in each valve region. In the 1.0*h* model, the highest maximum principal stress values were 1.2314 MPa, 0.4587 MPa, and 0.4427 MPa in the upper, mid, and lower regions, respectively. As the valve height increased, the stress curve for the upper region shifted downward (Fig. 5B), while the stress curve for the middle region shifted upward (Fig. 5C). In the

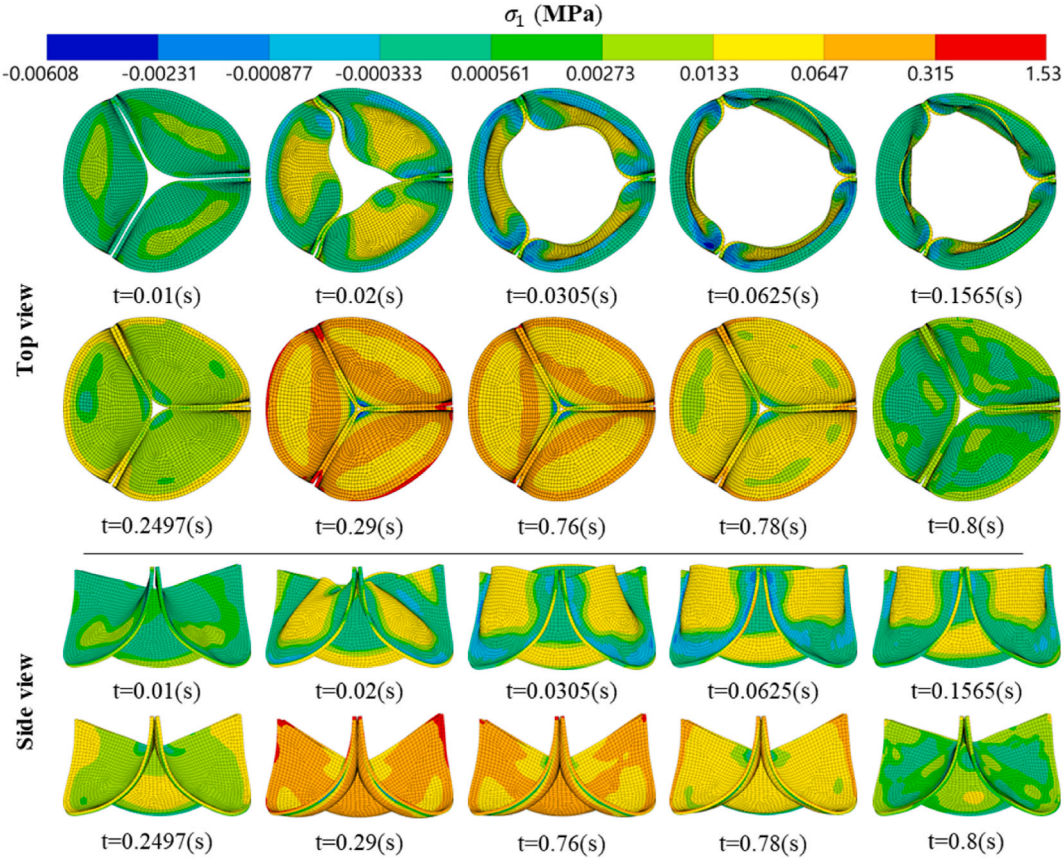

Fig. 3. The contour plot of the maximum principal stress (σ_1) in the original valve model (1.0*h* model).

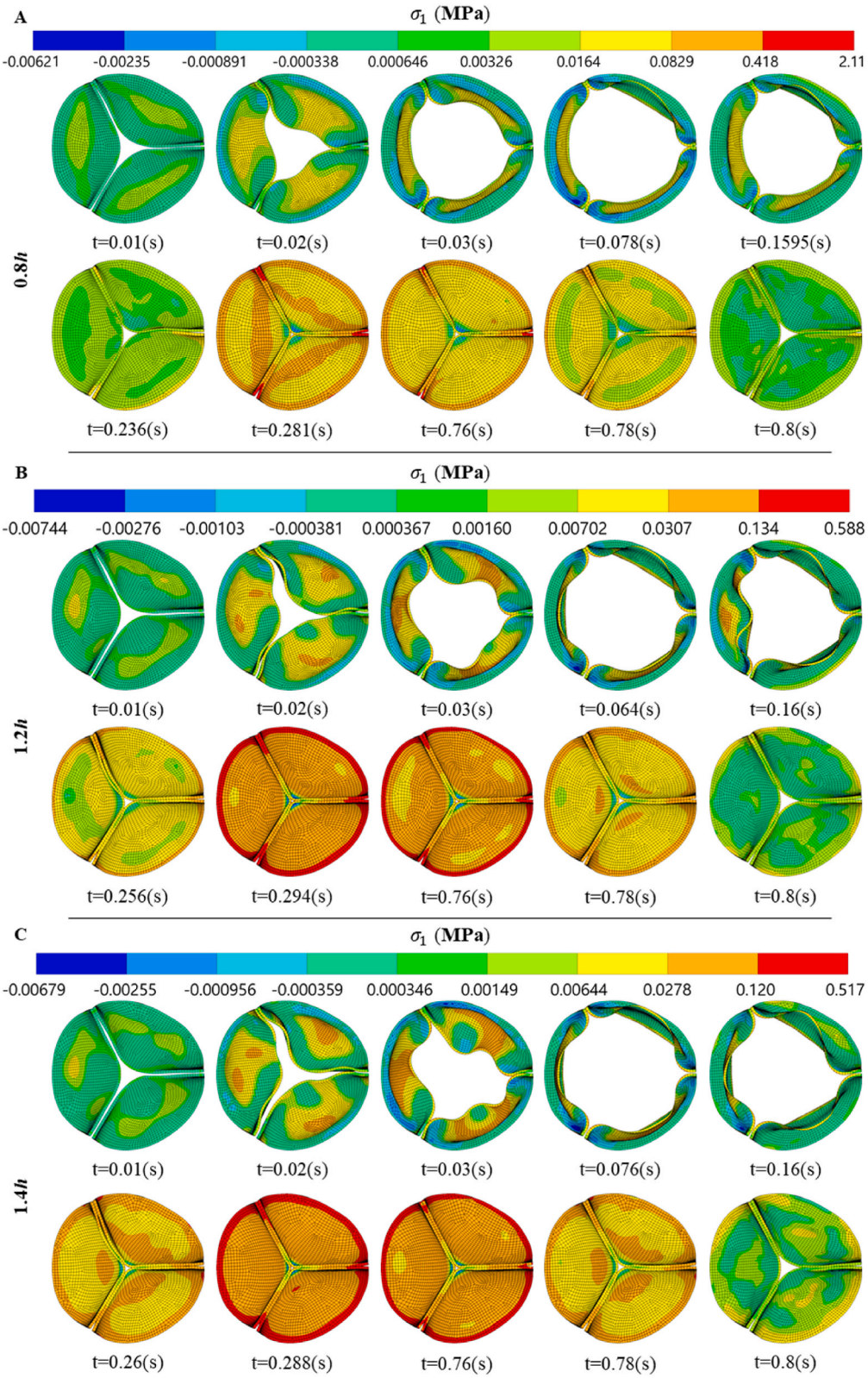

Fig. 4. Maximum principal stress (σ_1) contour plot of: **A)** 0.8*h*, **B)** 1.2*h*, and **C)** 1.4*h* models (0.8x, 1.2x and 1.4x models compared to the original height).

lower region, no significant trend was observed in the stress curve along the strut height (Fig. 5D).

The highest σ_1 value over the full cardiac cycle is summarized in Table 3, and values for each region are presented in Table S2. These results suggest that as the valve height increases, the region with the highest σ_1 shifts from the upper to the middle region. This implies that there exists an optimal valve height where the highest stress difference between the upper and middle regions is minimized. For example, the 1.2*h* model showed a 61.88% decrease in the highest stress value, whereas the 0.8*h* model exhibited a 35.52% increase in the highest stress value compared with 1.2032 MPa in the 1.0*h* model.

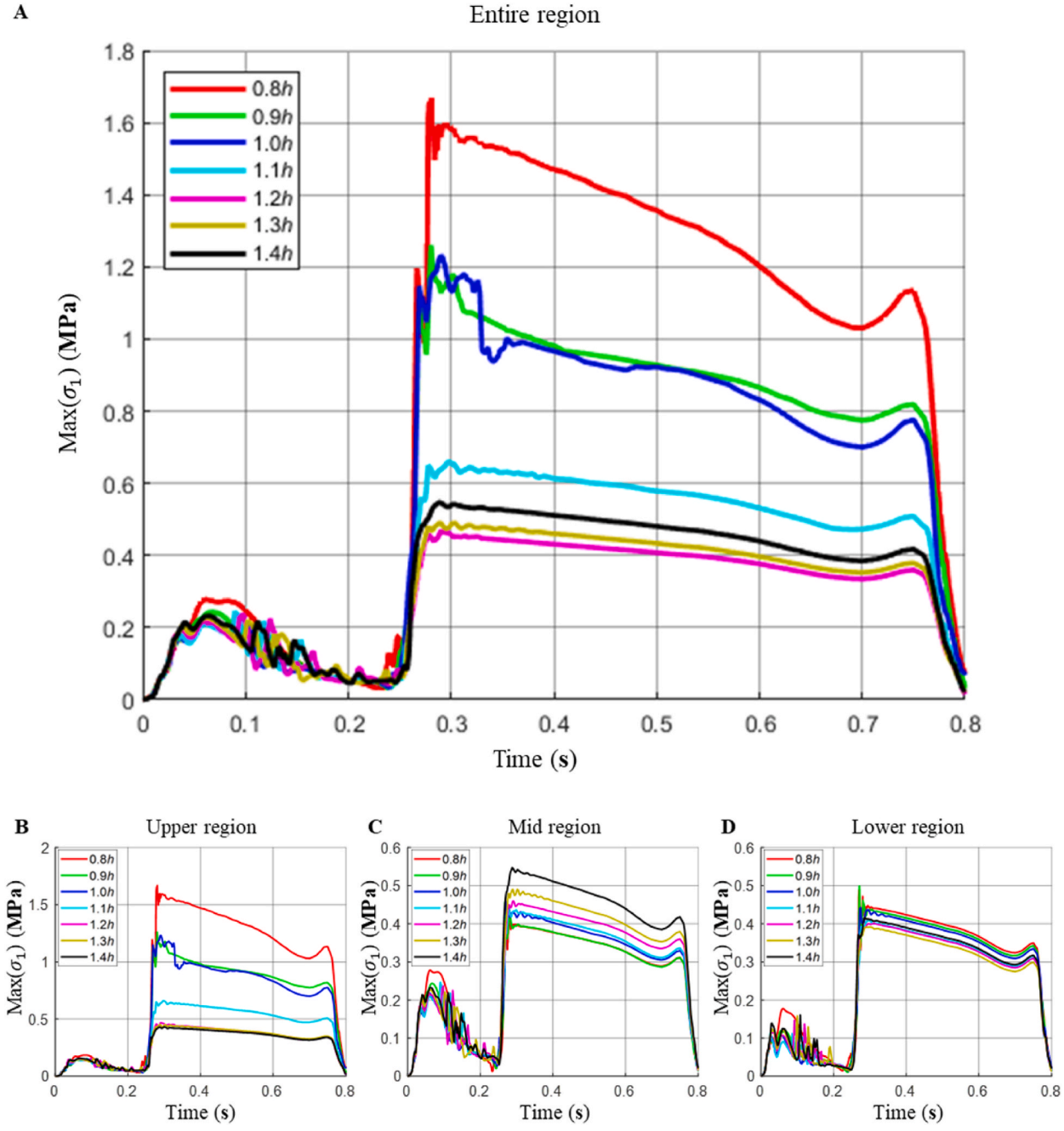

Fig. 5. Transient highest maximum principal stress (σ_1) on: **A)** entire region, **B)** upper region, **C)** mid-region, and **D)** lower region of leaflet during a cardiac cycle according to valve height.

4. Discussion

Bioprosthetic valves are primarily implanted in older patients because they eliminate the obligatory use of anticoagulant and cover the life expectancy, despite their shorter longevity compared with that of a mechanical valve [34]. However, the use of bioprosthetic valves has been steadily increasing, even in relatively young patients, considering the benefits of avoiding lifelong anticoagulation therapy and subsequent lifestyle modifications. Because the age of patients using bioprostheses is decreasing and patients tend to live longer, the durability of the bioprosthetic valve has become a significant goal to achieve [35].

Considering future valve reinterventions such as ViV TAVI, the new generation of bioprostheses is generally designed with shorter strut heights, and the height-to-diameter ratio of the valve is reduced from the typical value of 0.7 to approximately 0.41. However, when analyzing the distribution of mechanical stress, the strut height and leaflet coaptation angle are important geometric factors that eventually affect the longevity of the prosthesis. The flattened free edge angle in shorter valve struts may induce more stress and subsequent mechanical damage to the valve leaflet [36]. This underscores the importance of understanding how the geometrical shape of the valve affects the stress in the leaflets.

Our study results demonstrated that the maximum stress decreases when the valve strut height increases, as long as it does not exceed 1.2 times the original height. This suggests that the aortic valve we studied here is expected to experience reduced stress on the leaflet, reducing the likelihood of leaflet rupture. Short-strut valve may offer surgical convenience and reduce the risk of coronary artery occlusion. Nevertheless, we believe that an extended strut height, aimed at reducing the overall stress, can positively contribute to the durability of the bioprosthetic valve itself, potentially lowering the chances of reintervention.

Several limitations should be addressed in the simulation conducted in this study. First, it did not consider the compliance of the aortic sinus. Marom et al. [17] demonstrated that commissure stress is higher with compliant sinuses than that with rigid sinuses, Second, the complex geometry of the bioprosthesis, including the leaflet, stent, and skirt, was not considered, and hence, the compliance of the stent was not included. A previous study has shown that the flexibility of the stent can reduce commissure stress [37]. Third, the simulation did not consider coronary blood flow, which could affect leaflet behavior during cardiac pulsation. Fourth, the study focused solely on leaflet tear. Valve failure results from a complex, multifactorial process involving factors like calcification, thrombus formation, pannus, and more. Nevertheless, tear analysis is crucial, and this study can be valuable in future fatigue analysis, which is mechanically related to structural valve degeneration, if proper fatigue data are available. Finally, statistical variation was not considered in material properties of leaflet and blood and hemodynamic boundary conditions. Instead, we used representative values from normal subject group like other previous studies [15–18] since the normal values can be used later as a reference for future comparison with pathological cases.

5. Conclusion

The fluid structure interaction simulations of a bioprosthetic valve were performed to evaluate the stress distribution, EOA, valve opening area, stroke volume, and leakage volume, with different strut height. Especially, this study focused on how the strut height changes the stress distribution in the leaflet that is responsible for a leaflet tear. According to the simulation results, a bioprosthetic aortic valve with a slightly longer strut height exhibited a decrease in the maximum mechanical stress and an increase in the valve opening area compared with those of the standard model, and hence it is expected to have prolonged life span of the valve. The trend in new generation bioprosthetic valve is to shorten the strut height, with consideration for future valve reintervention. However, since this trend can increase the maximum stress and reduce the number of allowable cycles to fatigue failure, shortening the height of the valve too much may negatively affect valve durability and hence needs to be carefully considered in future valve design.

Further studies are required to overcome the limitations of this work. First, previous computational studies have shown that considering the compliance of the aortic sinus tends to increase the stress on the leaflet commissure [17], while considering the compliance of stent tends to decrease stress [37]. The combined effect of the compliance of both sinus and stent needs to be investigated. Second, inclusion of the coronary artery might reflect more realistic geometric environment and it is expected that non-symmetric hemodynamic behavior of the valve would be pronounced and hence affect the stress distribution on the leaflet. Lastly, fatigue analysis should also be performed in the future using appropriate fatigue data of bovine pericardium.

Funding

This research was supported by the Basic Science Research Program through the National Research Foundation of Korea (NRF), funded by the Ministry of Education (2019R1C1C1002502). This research was supported by mid-career researcher program (NRF-2022R1A2C2011266) through the NRF(National Research Foundation of Korea).

Ethical statement

This is an article reporting on computational simulations; neither animals nor human subjects are involved in this study. The requirement for approval of Institutional Review Board or Ethics Committee was waived owing to its experimental nature of this study.

Data availability statement

The data supporting the findings of present study are available from the corresponding author upon reasonable request. Detailed

methods are described in the Supplemental Material.

CRediT authorship contribution statement

Yongwoo Kim: Writing – original draft, Visualization, Validation, Methodology, Investigation, Formal analysis, Data curation. **Won Kyung Pyo:** Writing – review & editing, Writing – original draft, Visualization, Validation, Investigation. **Wan Kee Kim:** Project administration, Investigation. **Ga-Young Suh:** Writing – review & editing, Validation, Investigation. **Keonwook Kang:** Writing – review & editing, Validation, Supervision, Methodology, Funding acquisition, Formal analysis, Conceptualization. **Seung Hyun Lee:** Writing – review & editing, Supervision, Resources, Project administration, Funding acquisition, Conceptualization.

Declaration of competing interest

The authors declare that they have no known competing financial interests or personal relationships that could have appeared to influence the work reported in this paper.

Appendix A. Supplementary data

Supplementary data to this article can be found online at https://doi.org/10.1016/j.heliyon.2024.e27310.

References

[1] C.M. Otto, et al., ACC/AHA guideline for the management of patients with valvular heart disease: executive summary: a report of the American college of cardiology/American heart association joint committee on clinical practice guidelines, Circulation 143 (5) (2020) e35–e71, 2021.
[2] A. Vahanian, et al., 2021 ESC/EACTS Guidelines for the management of valvular heart disease, Eur. Heart J. 43 (7) (2022) 561–632.
[3] B. Medalion, et al., Aortic valve replacement: is valve size important? J. Thorac. Cardiovasc. Surg. 119 (5) (2000) 963–974.
[4] N. Hanayama, et al., Patient prosthesis mismatch is rare after aortic valve replacement: valve size may be irrelevant, Ann. Thorac. Surg. 73 (6) (2002) 1822–1829.
[5] A.N. Azadani, et al., Effect of transcatheter aortic valve size and position on valve-in-valve hemodynamics: an in vitro study, J. Thorac. Cardiovasc. Surg. 153 (6) (2017) 1303–1315.e1.
[6] O.M. Rotman, et al., Novel polymeric valve for transcatheter aortic valve replacement applications: in vitro hemodynamic study, Ann. Biomed. Eng. 47 (1) (2019) 113–125.
[7] M.S. Sacks, D.B. Smith, Effects of accelerated testing on porcine bioprosthetic heart valve fiber architecture, Biomaterials 19 (11–12) (1998) 1027–1036.
[10] T.M. Koch, et al., Aortic valve leaflet mechanical properties facilitate diastolic valve function, Comput. Methods Biomech. Biomed. Eng. 13 (2) (2010) 225–234.
[11] K. Li, W. Sun, Simulated thin pericardial bioprosthetic valve leaflet deformation under static pressure-only loading conditions: implications for percutaneous valves, Ann. Biomed. Eng. 38 (8) (2010) 2690–2701.
[12] S. Loerakker, et al., Effects of valve geometry and tissue anisotropy on the radial stretch and coaptation area of tissue-engineered heart valves, J. Biomech. 46 (11) (2013) 1792–1800.
[13] K.J. Grande-Allen, et al., Finite-element analysis of aortic valve-sparing: influence of graft shape and stiffness, IEEE (Inst. Electr. Electron. Eng.) Trans. Biomed. Eng. 48 (6) (2001) 647–659.
[14] H. Kim, et al., Dynamic simulation of bioprosthetic heart valves using a stress resultant shell model, Ann. Biomed. Eng. 36 (2) (2008) 262–275.
[15] K. Dumont, et al., Validation of a fluid–structure interaction model of a heart valve using the dynamic mesh method in fluent, Comput. Methods Biomech. Biomed. Eng. 7 (3) (2004) 139–146.
[16] S.C. Shadden, M. Astorino, J.-F. Gerbeau, Computational analysis of an aortic valve jet with Lagrangian coherent structures, Chaos: An Interdiscipl. J. Nonlinear Sci. 20 (1) (2010) 017512.
[17] G. Marom, et al., A fluid–structure interaction model of the aortic valve with coaptation and compliant aortic root, Med. Biol. Eng. Comput. 50 (2) (2012) 173–182.
[18] W. Mao, K. Li, W. Sun, Fluid–structure interaction study of transcatheter aortic valve dynamics using smoothed particle hydrodynamics, Cardiovasc. Eng. Technol. 7 (4) (2016) 374–388.
[19] Y. Chen, H. Luo, A computational study of the three-dimensional fluid–structure interaction of aortic valve, J. Fluid Struct. 80 (2018) 332–349.
[20] G. Luraghi, et al., Evaluation of an aortic valve prosthesis: fluid-structure interaction or structural simulation? J. Biomech. 58 (2017) 45–51.
[21] M.-C. Hsu, et al., Fluid–structure interaction analysis of bioprosthetic heart valves: significance of arterial wall deformation, Comput. Mech. 54 (2014) 1055–1071.
[22] M.S. Sacks, C. Chuong, Orthotropic mechanical properties of chemically treated bovine pericardium, Ann. Biomed. Eng. 26 (5) (1998) 892–902.
[23] H. Tam, et al., Fixation of bovine pericardium-based tissue biomaterial with irreversible chemistry improves biochemical and biomechanical properties, J. Cardiovasc. Transl. Res. 10 (2) (2017) 194–205.
[24] P. Zioupos, J. Barbenel, J. Fisher, Anisotropic elasticity and strength of glutaraldehyde fixed bovine pericardium for use in pericardial bioprosthetic valves, J. Biomed. Mater. Res. 28 (1) (1994) 49–57.
[25] A. Caballero, et al., Evaluation of transcatheter heart valve biomaterials: biomechanical characterization of bovine and porcine pericardium, J. Mech. Behav. Biomed. Mater. 75 (2017) 486–494.
[26] C. Capelli, et al., Patient-specific simulations of transcatheter aortic valve stent implantation, Med. Biol. Eng. Comput. 50 (2012) 183–192.
[27] J. De Hart, et al., A computational fluid-structure interaction analysis of a fiber-reinforced stentless aortic valve, J. Biomech. 36 (5) (2003) 699–712.
[28] F. De Vita, M. De Tullio, R. Verzicco, Numerical simulation of the non-Newtonian blood flow through a mechanical aortic valve: non-Newtonian blood flow in the aortic root, Theor. Comput. Fluid Dynam. 30 (2016) 129–138.
[29] J.R. Mitchell, J.-J. Wang, Expanding application of the Wiggers diagram to teach cardiovascular physiology, Adv. Physiol. Educ. 38 (2) (2014) 170–175.
[30] D. Perić, D. Owen, Computational model for 3-D contact problems with friction based on the penalty method, Int. J. Numer. Methods Eng. 35 (6) (1992) 1289–1309.
[31] Standardization, I.O.f., ISO 5840, Cardiovascular Implants – Cardiac Valve Prostheses.
[32] C. Dal Lin, et al., Carpentier-edwards Magna ease versus Magna valves: a comparison of in-vitro valve hydrodynamic performance, J. Heart Valve Dis. 21 (1) (2012) 112.

[33] M. Ugur, et al., Comparison of early hemodynamic performance of 3 aortic valve bioprostheses, J. Thorac. Cardiovasc. Surg. 148 (5) (2014) 1940–1946.
[34] R.A. Nishimura, et al., AHA/ACC guideline for the management of patients with valvular heart disease, Circulation 129 (23) (2014) e521–e643, 2014.
[35] M. Piepiorka-Broniecka, et al., NOAC versus warfarin in the treatment of atrial fibrillation during the first three months after bioprosthetic aortic valve replacement, Cardiol. J. 29 (2) (2022) 355–357.
[36] I. Vesely, The evolution of bioprosthetic heart valve design and its impact on durability, Cardiovasc. Pathol. 12 (5) (2003) 277–286.
[37] G.W. Christie, B.G. Barratt-Boyes, On stress reduction in bioprosthetic heart valve leaflets by the use of a flexible stent, J. Card. Surg. 6 (4) (1991) 476–481.